Large-scale structure in absorption: gas within and around galaxy voids

Nicolas Tejos,[1]⋆ Simon L. Morris,[1] Neil H. M. Crighton,[2] Tom Theuns,[1] Gabriel Altay[1] and Charles W. Finn[1]

[1]*Department of Physics, Durham University, South Road, Durham DH1 3LE*
[2]*Max Planck Institute for Astronomy, Königstuhl 17, D-69117 Heidelberg, Germany*

ABSTRACT

We investigate the properties of the H I Lyα absorption systems (Lyα forest) *within* and *around* galaxy voids at $z \lesssim 0.1$. We find a significant excess (>99 per cent confidence level, c.l.) of Lyα systems at the edges of galaxy voids with respect to a random distribution, on $\sim 5\,h^{-1}$ Mpc scales. We find no significant difference in the number of systems inside voids with respect to the random expectation. We report differences between both column density ($N_{\rm HI}$) and Doppler parameter ($b_{\rm HI}$) distributions of Lyα systems found inside and at the edge of galaxy voids at the $\gtrsim 98$ and $\gtrsim 90$ per cent c.l., respectively. Low-density environments (voids) have smaller values for both $N_{\rm HI}$ and $b_{\rm HI}$ than higher density ones (edges of voids). These trends are theoretically expected and also found in Galaxies-Intergalactic Medium Interaction Calculation (GIMIC), a state-of-the-art hydrodynamical simulation. Our findings are consistent with a scenario of *at least* three types of Lyα systems: (1) containing embedded galaxies and so directly correlated with galaxies (referred to as 'halo-like'), (2) correlated with galaxies only because they lie in the same overdense large-scale structure (LSS) and (3) associated with underdense LSS with a very low autocorrelation amplitude ($\approx$random) that are not correlated with luminous galaxies. We argue that the latter arise in structures still growing linearly from the primordial density fluctuations inside galaxy voids that have not formed galaxies because of their low densities. We estimate that these underdense LSS absorbers account for 25–30 ± 6 per cent of the current Lyα population ($N_{\rm HI} \gtrsim 10^{12.5}$ cm^{-2}), while the other two types account for the remaining 70–75 ± 12 per cent. Assuming that *only* $N_{\rm HI} \geq 10^{14}$ cm^{-2} systems have embedded galaxies nearby, we have estimated the contribution of the 'halo-like' Lyα population to be ≈ 12–15 ± 4 per cent and consequently ≈ 55–60 ± 13 per cent of the Lyα systems to be associated with the overdense LSS.

Key words: galaxies: formation – intergalactic medium – quasars: absorption lines – large-scale structure of Universe.

1 INTRODUCTION

The intergalactic medium (IGM) hosts the main reservoirs of baryons at all epochs (see Prochaska & Tumlinson 2009 for a review). This is supported by both observations (e.g. Fukugita, Hogan & Peebles 1998; Fukugita & Peebles 2004; Shull, Smith & Danforth 2011) and simulations (e.g. Cen & Ostriker 1999; Theuns et al. 1999; Davé et al. 2010). Efficient feedback mechanisms that expel material from galaxies to the IGM are required to explain the statistical properties of the observed galaxies (e.g. Baugh et al. 2005; Bower et al. 2006; Schaye et al. 2010). Given that galaxies are formed by accreting gas from the IGM, a continuous interplay between the IGM and galaxies is then in place. Consequently, understanding the relationship between the IGM and galaxies is key to understanding galaxy formation and evolution. This has been recognized since the earliest *Hubble Space Telescope* (*HST*) spectroscopy of quasi-stellar objects (QSOs), where the association between low-z IGM absorption systems and galaxies was investigated for the first time (e.g. Morris et al. 1993; Spinrad et al. 1993; Morris & van den Bergh 1994; Lanzetta et al. 1995; Stocke et al. 1995).

The large-scale environment in which matter resides is also important, as it is predicted (e.g. Borgani et al. 2002; Padilla et al. 2009) and observed (e.g. Lewis et al. 2002; Lopez et al. 2008; Padilla, Lambas & González 2010) to have non-negligible effects on the gas and galaxy properties. Given that baryonic matter is expected to fall into the considerably deeper gravitational potentials of dark matter, the IGM gas and galaxies are expected to be

predominantly found at such locations forming the so-called 'cosmic web' (Bond, Kofman & Pogosyan 1996). Identification of large-scale structures (LSS) like galaxy clusters, filaments or voids and their influence over the IGM and galaxies is then fundamental to a complete picture of the IGM/galaxy connection and its evolution over cosmic time.

With the advent of big galaxy surveys such as the 2dF (Colless et al. 2001) or the Sloan Digital Sky Survey (SDSS; Abazajian et al. 2009), it has been possible to directly observe the nature and extent of the distribution of stellar matter in the local Universe. Galaxies tend to lie in the filamentary structure which simulations predict; however, very little is known about the *actual* gas distribution at low *z*. In this work, we focus on the study of H I Lyα (hereafter referred simply as Lyα) absorption systems found *within* and *around* galaxy voids at $z \lesssim 0.1$.

Galaxy voids are the best candidates to start our statistical study of LSS in absorption. Voids account for up to 60–80 per cent of the volume of the universe at $z = 0$ (e.g. Aragón-Calvo, van de Weygaert & Jones 2010; Pan et al. 2012). Some studies have suggested that when a minimum density threshold is reached, voids grow in a spherically symmetric way (e.g. Regos & Geller 1991; van de Weygaert & van Kampen 1993). This suggests that voids have a relatively simple geometry, which makes them comparatively easy to define and identify from current galaxy surveys (although see Colberg et al. 2008, for a discussion on different void finder algorithms). Galaxy voids are a unique environment in which to look for evidence of early (or even primordial) enrichment of the IGM (e.g. Stocke et al. 2007). It is interesting that galaxy voids are present even in the distribution of low-mass galaxies (e.g. Peebles 2001; Tikhonov & Klypin 2009) and so there must be mechanisms that prevent galaxies from forming in such low-density environments.

Previous studies of Lyα absorption systems associated with voids at low *z* have relied on a 'nearest galaxy distance' (NGD) definition (e.g. Penton, Stocke & Shull 2002; Stocke et al. 2007; Wakker & Savage 2009). In order to have a clean definition of void absorbers the NGD must be large, leading to small samples. For instance, Penton et al. (2002) found only eight void absorbers (from a total of 46 systems) defined as being located at $>3\,h_{70}^{-1}$ Mpc from the nearest $\geq L^*$ galaxy. Wakker & Savage (2009) found 17 void absorbers (from a total of 102) based on the same definition. Stocke et al. (2007) had to relax the previous limit to $>1.4\,h_{70}^{-1}$ Mpc in order to find 61 void absorbers (from a total of 651 systems), although only 12 were used in their study on void metallicities. Note that a low NGD limit (of $1.4\,h_{70}^{-1}$ Mpc) could introduce some contamination of not-void absorbers. This is because filaments in the 'cosmic web' are expected to be a couple of Mpc in radius (Aragón-Calvo et al. 2010; Bond, Strauss & Cen 2010; González & Padilla 2010). Considering the Local Group as an example, being $1.4\,h_{70}^{-1}$ Mpc away from either the Milky Way or Andromeda cannot be considered as being in a galaxy void. On the other hand, given that there is a population of galaxies inside voids (e.g. Rojas et al. 2005; Park et al. 2007; Kreckel et al. 2011), the NGD definition could also miss some 'real' void absorbers relatively close to bright isolated galaxies. In fact, Wakker & Savage (2009) found that there may be no void absorbers in their sample (based on the NGD definition) if the luminosity limit to the closest galaxy is reduced to $0.1L^*$. Note, however, that their sample is very local ($z \leq 0.017$ or $\lesssim 70\,h_{70}^{-1}$ Mpc away), and it might be biased because of the local overdensity to which our Local Group belongs.

In this work we use a different approach to define void absorption systems. We based our definition on current galaxy void catalogues (typical radius of $>14\,h_{70}^{-1}$ Mpc), defining void absorbers as those located inside such galaxy voids. This leads to larger samples of well-identified void absorbers compared to previous studies. Moreover, this approach allows us to define a sample of absorbers located at the very edges of voids, which can be associated with walls, filaments and nodes, allowing us to get some insights in the distribution of gas in the 'cosmic web' itself. This definition is different from the NGD-based ones and it focuses on the 'large-scale' ($\gtrsim 10$ Mpc) relationship between Lyα forest systems and galaxies. The results from this work will offer a good complement to previous studies based on 'local' scales ($\lesssim 2$ Mpc).

Our paper is structured as follows. The catalogues of both Lyα systems and galaxy voids that we used in this work are described in Section 2. Definition of our LSS in absorption samples and the observational results are presented in Section 3. We compare our observational results with a recent cosmological hydrodynamical simulation in Section 4. We discuss our findings in Section 5 and summarize them in Section 6. A check for systematic effects and biases that could be present in our data analysis is presented in Appendix A. All distances are in comoving coordinates assuming $H_0 = 100\,h\,\mathrm{km\,s^{-1}\,Mpc^{-1}}$, $h = 0.71$, $\Omega_{\mathrm{m}} = 0.27$, $\Omega_\Lambda = 0.73$, $k = 0$ cosmology unless otherwise stated. This cosmology was chosen to match the one adopted by Pan et al. (2012) (D. Pann, private communication; see Section 2.2).

2 DATA

2.1 Gas in absorption

We use QSO absorption line data from the Danforth & Shull (2008, hereafter DS08) catalogue, which is the largest high-resolution ($R \equiv \Delta\lambda/\lambda \approx 30\,000$–$100\,000$), low-*z* IGM sample to date.[1] Briefly, the catalogue lists 651 Lyα absorption systems at $z_{\mathrm{abs}} \leq 0.4$, with associated metal lines [O VI, N V, C IV, C III, Si IV, Si III and Fe III; when the spectral coverage and signal-to-noise ratio (S/N) allowed their observation], taken from 28 active galactic nuclei (AGNs) observed with both the Space Telescope Imaging Spectrograph (STIS; Woodgate et al. 1998) on the *HST* and the *Far Ultraviolet Spectroscopic Explorer* (*FUSE*; Moos et al. 2000). The systems are characterized by their rest-frame equivalent widths (W_{r}), or upper limits on W_{r}, for each individual transition. Column densities (N_{HI}) and Doppler parameters (b_{HI}) were inferred using the apparent optical depth (AOD) method (Savage & Sembach 1991) and/or Voigt profile line fitting. In particular for the Lyα transition, a curve-of-growth (COG) solution was used when other Lyman series lines were available (see also Section A2). We refer the reader to DS08 (and references therein) for further description and discussion.

In order to identify absorbing gas associated with LSS [drawn from the SDSS Data Release 7 (DR7)], we use a subsample of the DS08 AGN sightlines that intersect the SDSS volume (PG 0953+414, Ton 28, PG 1116+215, PG 1211+143, PG 1216+069, 3C 273, Q 1230+0115, PG 1259+593, NGC 5548, Mrk 1383 and PG 1444+407; see Table 1). Despite the fact that PG 1216+069 spectrum has a poor quality, it is still possible to find strong systems in it, and so we decided not to exclude it from the

---

[1] We note that after this paper was submitted, a new preprint by Tilton et al. (2012) appeared with an updated version of the DS08 catalogue.

Table 1. IGM sightlines from DS08 that intersect the SDSS survey.

Sightline	RA (J2000)	Dec. (J2000)	z_{AGN}	S/N[a]
PG 0953+414	09 56 52.4	+41 15 22	0.234 10	14
Ton 28	10 04 02.5	+28 55 35	0.329 70	9
PG 1116+215	11 19 08.6	+21 19 18	0.176 50	18
PG 1211+143	12 14 17.7	+14 03 13	0.080 90	30
PG 1216+069	12 19 20.9	+06 38 38	0.331 30	3
3C 273	12 29 06.7	+02 03 09	0.158 34	35
Q 1230+0115	12 30 50.0	+01 15 23	0.117 00	12
PG 1259+593	13 01 12.9	+59 02 07	0.477 80	12
NGC 5548	14 17 59.5	+25 08 12	0.017 18	13
Mrk 1383	14 29 06.6	+01 17 06	0.086 47	16
PG 1444+407	14 46 45.9	+40 35 06	0.267 30	10

[a]Median *HST*/STIS S/N per 2-pixel resolution element in the 1215–1340 Å range (C. Danforth, private communication). The expected minimum equivalent width, W_{min}, at a confidence level of cl corresponding to a given S/N can be estimated from $W_{min} = \frac{cl \times \lambda}{R(S/N)}$, where R is the spectral resolution (e.g. see DS08).

sample (this inclusion does not affect our results; see Section 3.1).[2] We use the rest of the sightlines in the DS08 catalogue to derive the general properties of the average absorber for comparison (see Section A1).

In our analysis, we focus on statistical comparisons of the H I properties in different LSS environments. Metal systems have smaller redshift coverage and lower number densities than Lyα absorbers. Consequently, we do not aim to draw statistical conclusions from them. We intend to pursue metallicity studies in future work.

2.2 Galaxy voids

We use a recently released galaxy-void catalogue from SDSS DR7 galaxies (Pan et al. 2012, hereafter P12), which is the largest galaxy-void sample to date. Hereafter we will use the term void to mean galaxy-void unless otherwise stated. P12 identified $\gtrsim 1000$ cosmic voids using the VOIDFINDER algorithm described by Hoyle & Vogeley (2002), with redshifts in the range of $0.01 \lesssim z \lesssim 0.102$. To summarize, it first uses a nearest neighbour algorithm on a volume-limited galaxy survey. Galaxies whose third nearest neighbour distance is greater than $6.3\,h^{-1}$ Mpc are classified as potential void galaxies, whereas the rest are classified as *wall* galaxies. Void regions are identified by looking for maximal empty spheres embedded in the *wall* galaxy sample. These individual void spheres have radii in the range of $10 < R_{void} \lesssim 25\,h^{-1}$ Mpc, with mean radius $\langle R_{void} \rangle \approx 13\,h^{-1}$ Mpc. The minimum radius of $10\,h^{-1}$ Mpc for the void spheres was imposed. Only galaxies with spectroscopic redshifts were used and therefore we expect the uncertainties in the void centres and radii to be small ($\lesssim 1$ Mpc; we will discuss the effects of peculiar velocities in Section 3.1). Independent void regions are defined by combining all the adjacent spheres that share more than 10 per cent of their volume with another. Void galaxies are defined as those galaxies that lie within a void region. We refer the reader to P12 for further description and discussion.

In our analysis, for simplicity, we use the individual spheres as separate voids instead of using the different independent void re-

[2] We note that Chen & Mulchaey (2009) have presented an Lyα absorption system list along PG 1216+069 sightline at a better sensitivity than that of DS08. In order to have an homogeneous sample, we did not include these new data in our analysis however.

gions. This choice has the following advantages. First, it allows us to use a perfectly spherical geometry, making it possible to characterize each void by just one number: its radius. Thus, we can straightforwardly scale voids with different sizes for comparison. Secondly, this approach allows us to identify regions at the very edges of the voids. P12 found that the number density of galaxies has a sharp peak at a distance $\approx R_{void}$ from the centre of the void spheres, a clear signature that walls are well defined (at least from the point of view of bright galaxies at low redshifts). This is also consistent with the predictions of linear gravitation theory (e.g. Icke 1984; Sheth & van de Weygaert 2004) and dark matter simulations (e.g. Benson et al. 2003; Colberg et al. 2005; Ceccarelli et al. 2006; P12). Therefore, by looking for absorption systems very close to the edge of voids, we expect to trace a different cosmic environment. Thirdly, using the individual void spheres securely identifies void regions. The void-edge sample on the other hand could be contaminated by void regions associated with the intersections of two void spheres. We checked that this is not the case though (see Section 3.2). This contamination should only reduce any possible difference between the two samples rather than enhance them. We also note that systematic uncertainties produced by assuming voids to be perfect spheres should also act to reduce any detected difference.

3 DATA ANALYSIS AND RESULTS

3.1 Number density of absorption systems around voids

We have cross-matched the IGM absorption line catalogue from DS08 (see Section 2.1) with the void catalogue from P12 (see Section 2.2). A total of 106 Lyα absorption systems were found in the 11 sightlines that intersect the void sample volume (i.e. those with $0.01 \leq z_{abs} \leq 0.102$).

We first look for a possible difference in the number density of Lyα systems as a function of the distance to voids. We take two approaches. First, we define X as the three-dimensional distance between an absorption system and the closest void centre in R_{void} units, so

$$X \equiv \min_{sample} \frac{s}{R_{void}}, \tag{1}$$

where s is the comoving distance between the centre of the closest void and the absorber. Thus, $0 \leq X < 1$ corresponds to absorption systems inside voids and $X > 1$ corresponds to absorption systems outside voids. A value of $X \approx 1$ corresponds to absorption systems around void edges as defined by the galaxy distribution.

The second approach defines D as the three-dimensional distance between an absorption system and the closest void edge in comoving h^{-1} Mpc, so

$$D \equiv \min_{sample} (s - R_{void})\,[h^{-1}\,\text{Mpc}]. \tag{2}$$

Negative D values correspond to absorption systems inside voids, while positive values correspond to absorbers outside voids. Values of $D \approx 0\,h^{-1}$ Mpc are associated with absorption systems around void edges as defined by the galaxy distribution.

Distances were calculated assuming the absorption systems to have no peculiar velocities with respect to the centre of the voids. Although this assumption might be realistic for gas inside voids, it might not be the case for gas residing in denser environments, where gas outflows from galaxies might dominate. However, some studies have suggested that the bulk of Lyα forest lines have little velocity offset with respect to galaxies (e.g. Theuns et al. 2002; Wilman
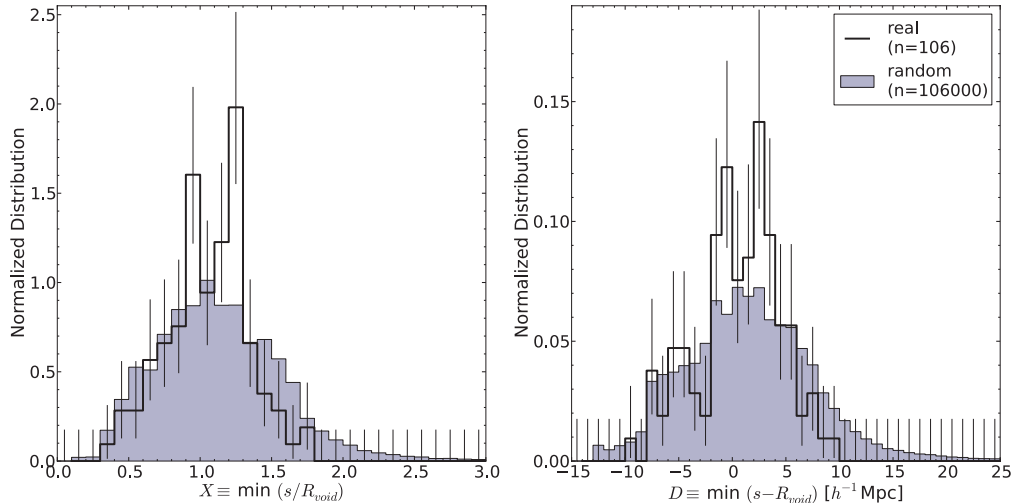
Figure 1. Normalized (in area) distribution of H I absorption systems as a function of X (left-hand panel; 0.1 binning) and D (right-hand panel; $1\,h^{-1}$ Mpc binning) for both real and random samples. Error bars correspond to the Poissonian uncertainty from the analytical approximation $\sigma_n^+ \approx \sqrt{n + 3/4} + 1$ and $\sigma_n^- \approx \sqrt{n - 1/4}$ (Gehrels 1986). Real and random distributions are different at a $\gtrsim 99.5$ per cent c.l. (see Section 3.1 for further details).

et al. 2007). As an example, a velocity difference of $\sim 200\,\mathrm{km\,s^{-1}}$ at redshift $z_{\rm abs} \lesssim 0.1$ would give an apparent distance shift of the order of $\sim 2\,h^{-1}$ Mpc, which is somewhat higher than but comparable to the systematic error of the void centre determination (given that void regions are not perfectly spherical as assumed here). Note that the uncertainty in the void centre is smaller than the uncertainty of a single galaxy because the void is defined by an average over many galaxies. As previously mentioned, such an uncertainty should not artificially create a false signal but rather should dilute any real difference.

Although the X and D coordinates are not independent, we decided to show our results using both. This has the advantage of testing the consistency of our results using two slightly differently motivated definitions. X is a scaled coordinate, good for stacking voids of different radii. It is also good for comparisons with some of the P12 results. D gives a direct measure of the actual distances involved, while still using $R_{\rm void}$. For convenience, results associated with the X definition will be shown normally in the text while results associated with the D definition will be shown in parenthesis: $X\,(D)$ format.

Fig. 1 shows the histogram of absorption systems as a function of X and D (left- and right-hand panels, respectively). In order to show the effects of the geometry of the survey, the random expectations are also shown (shaded distributions). To generate the random samples, we placed 1000 random absorption systems per real one, uniformly in the range $z_{\rm lim} < z_{\rm abs} \leq 0.102$ for each sightline, where $z_{\rm lim}$ corresponds to the maximum of 0.01 and the minimum observed redshift for a Lyα in that sightline. In this calculation, we have masked out spectral regions over a velocity window of $\pm 200\,\mathrm{km\,s^{-1}}$ around the position where strong Galactic absorption could have been detected (namely C I, C II, N V, O I, Si II, P III, S I, S II, Fe II and Ni II) *before* the random redshifts are assigned. A total of 106 000 random absorbers were generated. We observe a relative excess of absorption systems compared to the random expectation in the range of $X \simeq 0.9$–1.3 and/or $D \simeq -2$–$4\,h^{-1}$ Mpc. Assuming Poisson uncertainty, there were $61 \pm 8\ (65 \pm 8)^3$ ob-

---

[3] Results regarding distances from the centre of voids are presented in a $X\,(D)$ format (see Section 3.1). Reference to this footnote will be omitted hereafter.

served, while $\approx 38.3 \pm 0.2\ (42.4 \pm 0.2)$ were expected from the random distribution. This corresponds to an $\approx 3\sigma$ excess. Similarly, there is a significant ($\approx 3\sigma$) deficit of absorption systems at $X \gtrsim 1.3$ and/or $D \gtrsim 4\,h^{-1}$ Mpc, for which $17 \pm 4\ (19 \pm 4)$ systems were observed compared to the $33.9 \pm 0.2\ (34.1 \pm 0.2)$ randomly expected. We also checked that such an excess and deficit did not appear by chance in 1000 realizations, consistent with the <0.1 per cent probability of occurrence. No significant difference is found for systems at $X \lesssim 0.9$ and/or $D \lesssim -2\,h^{-1}$ Mpc, for which the $28 \pm 5\ (22 \pm 5)$ found are consistent with the random expectation of $33.4 \pm 0.2\ (29.0 \pm 0.2)$. The Kolmogorov–Smirnov (KS) test between the full unbinned samples gives an ≈ 0.3 per cent (0.5 per cent) probability that both the random and the real data come from the same parent distribution. We checked that no single sightline dominates the signal by removing each individual one and repeating the previous calculation. We also checked that masking out the spectral regions associated with possible Galactic absorption does not have an impact on our results as the same numbers (within the errors) are recovered when these regions are not excluded. These results hint at a well-defined gas structure around voids, possibly analogous to that seen in galaxies. The current data are not sufficient to confirm (at a high confidence level, c.l.) the reality of the apparent two-peaked shape seen in the real distributions however.

### 3.2 Definition of large-scale structure in absorption

We define three LSS samples observed in absorption.

(i) *Void absorbers*: those absorption systems with $X < 1$ and/or $D < 0\,h^{-1}$ Mpc. A total of 45 (45) void absorbers were found.

(ii) *Void-edge absorbers*: those absorption systems with $1 \leq X < 1.3$ and/or $0 \leq D < 4\,h^{-1}$ Mpc. A total of 44 (42) void-edge absorbers were found.

(iii) *Unclassified absorbers*: those absorption systems with $X \geq 1.3$ and/or $D \geq 4\,h^{-1}$ Mpc. A total of 17 (19) unclassified absorbers were found.

To be consistent with the galaxy-void definition, we use $X = 1$ and/or $D = 0\,h^{-1}$ Mpc as the limits between void and void-edge absorbers. The division between void-edge and unclassified absorbers was chosen to match the transition from the overdensity to the
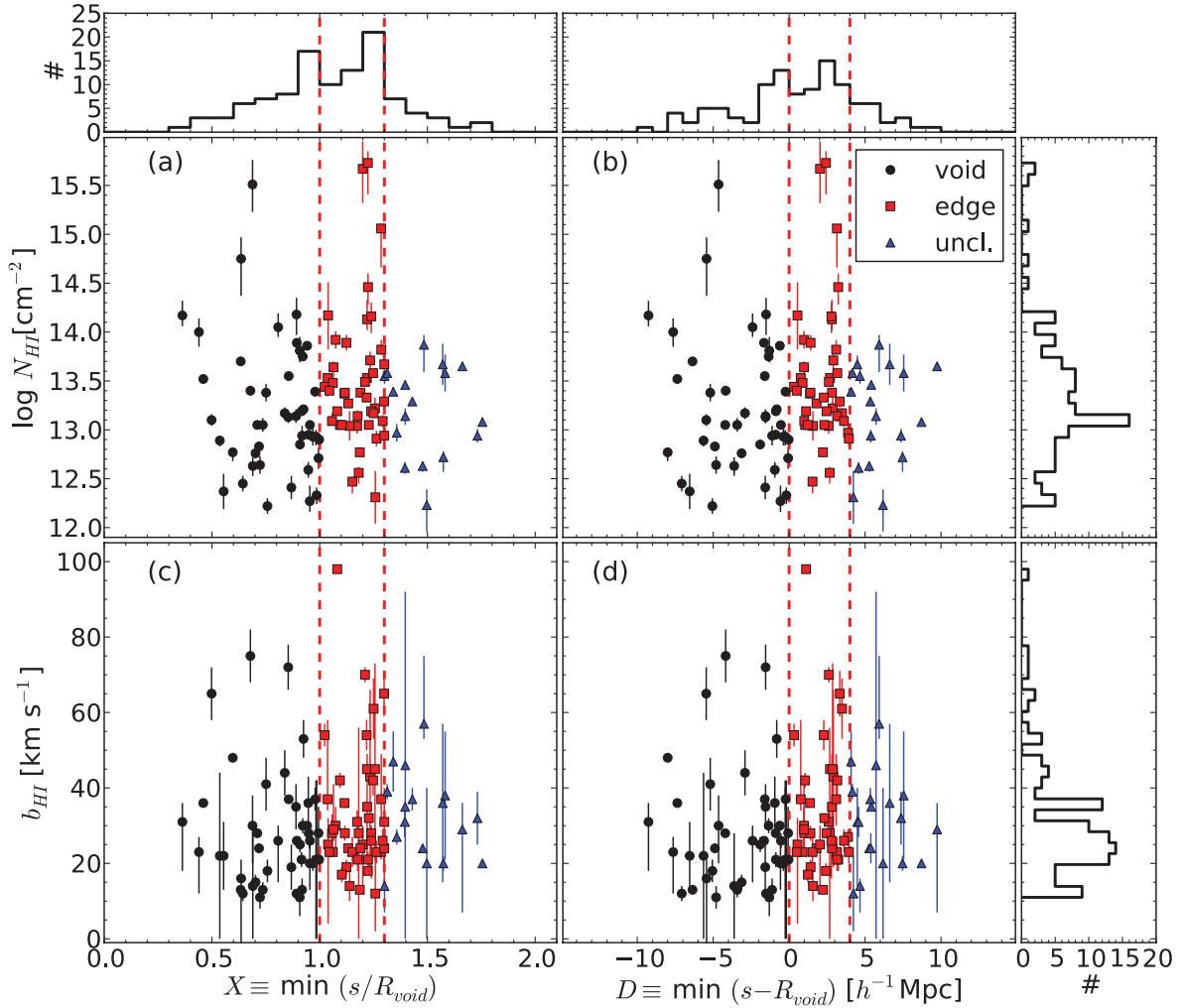
Figure 2. Panels (a) and (b) show the distribution of column densities of H I as a function of X and D, respectively. Panels (c) and (d) show the distribution of Doppler parameters as a function of X and D, respectively. Our LSS samples are shown by different colours/symbols: void (black circles), void-edge (red squares) and unclassified (blue triangles). Histograms are also shown around the main panels. Vertical red dashed lines show the limits of our LSS definitions (see Section 3.2).

underdensity of observed absorbers compared to the random expectation at $X > 1$ and/or $D > 0\,h^{-1}$ Mpc (see Fig. 1).

We have assumed here that the centre of galaxy voids will roughly correspond to the centre of gas voids; however, that does not necessarily imply that gas voids and galaxy voids have the same geometry. In fact, as we do not find a significant underdensity in the number of void absorbers with respect to the random expectation, it is not clear that such voids are actually present within the Lyα forest population. Of course, the fact that we do not detect this underdensity does not imply that the gas voids are not there. A better way to look at these definitions is by considering void absorbers as those found in galaxy underdensities (galaxy voids) and void-edge absorbers as those found in regions with a typical density of galaxies. We do not have a clear picture of what the unclassified absorbers correspond to. Unclassified absorbers are those lying at the largest distances from the *catalogued* voids, but this does not necessarily imply that they are associated with the highest density environments only. In fact, there could be high-density regions also located close to void-edges, at the intersection of the cosmic web filaments. Given that voids of radius $\lesssim 10\,h^{-1}$ Mpc are not present in the current catalogue, it is also likely that some of the unclassified absorbers are associated with low-density environments. Therefore, one interpre-

tation of unclassified absorbers could be as being a mixture of all kind of environments, including voids, void-edges and high-density regions.

We checked the robustness of these definitions by looking at the number of voids and void-edges which can be associated with a given absorber. In other words, for a given absorption system, we counted how many voids or void-edges could have been associated with it by taking simply $X \equiv s/R_{\rm void}$ or $D \equiv s - R_{\rm void}$ (in contrast to having taken the minimum values). Out of the 45 void absorbers, 41 are associated with only one void and four are associated with two voids, independently of the definition used (either X or D). Likewise, out of the 44 (42) void-edge absorbers, 31 (28) are associated with just one void-edge, 12 (13) are associated with two void-edges and 1 (1) is associated with three void-edges. This last system is located at $X = 1.04$ ($D = 0.55\,h^{-1}$ Mpc) and has $N_{\rm HI} = 10^{14.17 \pm 0.35}$ cm^{-2} and $b_{\rm HI} = 25^{+21}_{-7}$ km s^{-1} at a redshift of $z_{\rm abs} = 0.015\,33$. From these values the system does not seem to be particularly peculiar. Finding an association with more than two void-edges is not surprising as long as the filling factor of voids is not small.[4] Void absorbers have

[4] For reference, voids found by P12 have a filling factor of 62 per cent.

Table 2. General properties of our LSS samples.[a]

Sample	$\log(N_{HI} \, [\text{cm}^{-2}])$			$b_{HI} \, (\text{km s}^{-1})$	
	Mean	Median		Mean	Median
Void	13.21 ± 0.67 (13.21 ± 0.67)	13.05 (13.05)		28 ± 15 (28 ± 15)	25 (25)
Edge	13.50 ± 0.70 (13.52 ± 0.69)	13.38 (13.38)		33 ± 17 (34 ± 17)	28 (28)
Unclassified	13.20 ± 0.45 (13.17 ± 0.48)	13.36 (13.36)		33 ± 11 (31 ± 11)	32 (31)

[a]Results are presented in a X (D) format (see Section 3.1).

on average 1.1 ± 0.3 voids associated with them, with a median of 1. Void-edge absorbers have on average 1.3 ± 0.5 (1.4 ± 0.5) void-edges associated with them, with a median of 1 (1). These values give a median one-to-one association. Therefore, we conclude then that the LSS definitions used here are robust.

3.3 Properties of absorption systems in different large-scale structure regions

Fig. 2 shows the distribution of column densities and Doppler parameters as a function of both X and D. At first sight, no correlation is seen between N_{HI} or b_{HI} and distance to the centre of voids. Table 2 gives the mean and median values of $\log(N_{HI} \, [\text{cm}^{-2}])$ and b_{HI} for our void, void-edge and unclassified absorption systems. These results show consistency within 1σ between the three LSS samples.

A closer look at the problem can be taken by investigating the possible differences in the full N_{HI} and b_{HI} distributions of void, void-edge and unclassified absorbers.

3.3.1 Column density distributions

Fig. 3 shows the distribution of column density for the three different LSS samples defined above (see Section 3.2). The top panels show the normalized fraction of systems as a function of N_{HI} (arbitrary binning), whilst the bottom panels show the cumulative distributions (unbinned). We see from the top panels that this distribution seems to peak systematically at higher N_{HI} from void to void-edge and from void-edge to unclassified absorbers. We also observe a suggestion of a relative excess of weak systems ($N_{HI} \lesssim 10^{13} \, \text{cm}^{-2}$) in voids compared to those found in void-edges. This can also be seen directly in Fig. 2 (see panels a and b). The KS test gives a probability $P_{\text{void/edge}}^{\log N} \approx 2$ per cent (0.7 per cent) that void and void-edge absorbers come from the same parent distribution. This implies a $>2\sigma$ difference between these samples. No significant difference is found between voids or void-edges with unclassified absorbers, for which the KS test gives probabilities of $P_{\text{void/uncl.}}^{\log N} \approx 74$ per cent (66 per cent) and $P_{\text{edge/uncl.}}^{\log N} \approx 56$ per cent (24 per cent), respectively. These results can be understood by looking at the bottom panels of Fig. 3, as we see that the maximum difference between the void and void-edge absorber distributions is at $N_{HI} \lesssim 10^{13.8} \, \text{cm}^{-2}$. On the other hand, no big differences are observed at $N_{HI} \gtrsim 10^{13.8} \, \text{cm}^{-2}$. In fact, by considering just the systems at $N_{HI} < 10^{13.8} \, \text{cm}^{-2}$, the significance of the difference between void and void-edge absorbers is increased, with $P_{\text{void/edge}}^{\log N} \approx 0.9$ per cent (0.2 per cent). Likewise, at $N_{HI} \geq 10^{13.8} \, \text{cm}^{-2}$, void and void-edge absorber distributions agree at the ≈ 86 per cent (86 per cent) c.l. We, however, note that there were ≤ 10 systems per sample for this last comparison and therefore it is likely to be strongly affected by low number statistics.
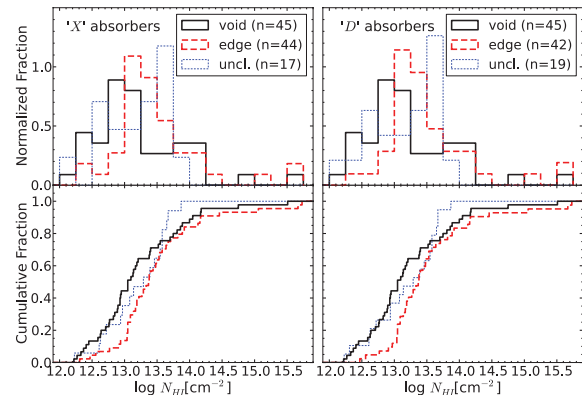
Figure 3. H I column density distribution for the three different LSS samples defined in this work (see Section 3.2): void absorbers (solid black lines), void-edge absorbers (red dashed lines) and unclassified absorbers (blue dotted lines). The top panels show the normalized distribution using arbitrary binning of 0.5 dex. The bottom panels show the cumulative distributions for the unbinned samples. The left- and right-hand panels correspond to absorbers defined using the X and D coordinates, respectively.

We also investigated possible differences between void, void-edge and unclassified absorbers and their complements (i.e. all the systems that were not classified as these: not-void, not-void-edge, not-unclassified). Not-voids correspond to the combination of void-edge and unclassified absorbers and so on. The KS gives probabilities of $P_{\text{void/not-void}}^{\log N} \approx 4$ per cent (4 per cent) and $P_{\text{edge/not-edge}}^{\log N} \approx 3$ per cent (0.6 per cent) implying that void and void-edge absorbers are somewhat inconsistent with their complements. On the other hand, the distribution of unclassified absorbers is consistent with the distribution of their complements with a KS probability of $P_{\text{uncl./not-uncl.}}^{\log N} \approx 64$ per cent (54 per cent). These results are summarized in Table 3.

3.3.2 Doppler parameter distributions

Fig. 4 shows the distribution of Doppler parameter for the three different LSS samples defined above (see Section 3.2). The top panels show the normalized fraction of systems as a function of b_{HI} (arbitrary binning), whilst the bottom panels show the cumulative distributions (unbinned). This figure suggests a relative excess of low-b_{HI} systems ($b_{HI} \lesssim 20 \, \text{km s}^{-1}$) in voids compared to those from void-edge and unclassified samples. A relative excess of unclassified absorbers compared to that of voids or void-edges at high-b_{HI} values ($b_{HI} \gtrsim 35 \, \text{km s}^{-1}$) is also suggested by the figure. The KS test gives a probability $P_{\text{void/edge}}^{b} \approx 8$ per cent (6 per cent) that void and void-edge absorbers come from the same parent distribution. This implies no detected difference between void and void-edge absorbers. Likewise, no significant difference is found between voids or void-edges with unclassified absorbers,

for which the KS test gives probabilities of $P^b_{\text{void/uncl.}} \approx 18$ per cent (17 per cent) and $P^b_{\text{edge/uncl.}} \approx 71$ per cent (75 per cent), respectively.

As before, we also investigated possible difference between LSS and their complements. In this case, void, void-edge or unclassified absorbers are not significantly different from their complements with KS probabilities of $P^b_{\text{void/not}-\text{void}} \approx 7$ per cent (7 per cent), $P^b_{\text{edge/not}-\text{edge}} \approx 20$ per cent (14 per cent) and $P^b_{\text{uncl./not}-\text{uncl.}} \approx 32$ per cent (32 per cent). These results are also summarized in Table 3.

3.4 Check for systematic effects

Given that the differences between void and void-edge samples are still at $<3\sigma$ c.l., we have investigated possible biases or systematic effects that could be present in our data analysis. In particular, we have investigated (1) possible differences in our subsample with respect to the whole DS08 sample, (2) the effect of the different characterization methods used by DS08 to infer the gas properties and (3) whether uniformity across our redshift range is present in our observables. A complete discussion is presented in Appendix A. From that analysis, we concluded that no important biases affect our results.

4 COMPARISON WITH SIMULATIONS

In this section, we investigate whether current cosmological hydrodynamical simulations can reproduce our observational results presented in Section 3. For this comparison, we use the Galaxies-Intergalactic Medium Interaction Calculation (GIMIC; Crain et al. 2009).Using initial conditions drawn from the Millennium Simulation (Springel et al. 2005), GIMIC follows the evolution of baryonic gas within five roughly spherical regions (radius between 18 and $25\,h^{-1}$ Mpc[5]) down to $z = 0$ at a resolution of $m_{\text{gas}} \approx 10^7\,h^{-1}\,\text{M}_\odot$. The regions were chosen to have densities deviating by $(-2, -1, 0, +1, +2)\sigma$ from the cosmic mean at $z = 1.5$, where σ is the rms mass fluctuation. The $+2\sigma$ region was additionally required to be centred on a rich cluster halo. Similarly although not imposed, the -2σ region is approximately centred on a sparse void. The rest of the Millennium Simulation volume is resimulated using only the dark matter particles at much lower resolution to account for the tidal forces. This approach gives GIMIC the advantage of probing a wide range of environments and cosmological features with a comparatively low computational expense.

GIMIC includes (i) a recipe for star formation designed to enforce a local Kennicutt–Schmidt law (Schaye & Dalla Vecchia 2008), (ii) stellar evolution and the associated delayed release of 11 chemical elements (Wiersma et al. 2009b), (iii) the contribution of metals to the cooling of gas in the presence of an imposed ultraviolet (UV) background (Wiersma, Schaye & Smith 2009a) and (iv) galactic winds that pollute the IGM with metals and can quench star formation in low-mass haloes (Dalla Vecchia & Schaye 2008). Note that GIMIC does not include feedback processes associated with AGN. For further details about GIMIC we refer the reader to Crain et al. (2009).

4.1 Simulated H I absorbers sample

In order to obtain the properties of the simulated H I absorption systems, we placed 1000 parallel sightlines within a cube of $20\,h^{-1}$ Mpc on a side centred in each individual GIMIC region at $z = 0$ (5000 sightlines in total). We have excluded the rest of the volume to avoid any possible edge effects. This roughly corresponds to 2.5 sightlines per square h^{-1} Mpc. Given this density, some sightlines could be tracing the same local LSS and therefore these are not fully independent. We consider this approach to offer a good compromise of having a large enough number of sightlines while not oversampling the limited GIMIC volumes.

We used the program SPECWIZARD[6] to generate synthetic normalized spectra associated with our sightlines using the method described by Theuns et al. (1998b). SPECWIZARD calculates the optical depth as a function of velocity along the line of sight, which is then converted to flux transmission as a function of wavelength for a given transition. We only used H I in this calculation. The spectra were convolved with an instrumental spread function (Gaussian) with a full width at half-maximum of $6.6\,\text{km s}^{-1}$ to match the resolution of the STIS/*HST* spectrograph.[7] In order to mimic the continuum fitting process in real spectra, we set the continuum level of each mock *noiseless* spectrum at the largest flux value after the convolution with the instrumental profile. Given that the lines are sparse at $z = 0$, there were almost always regions with no absorption and this last correction was almost negligible.

We used three different S/N values in order to represent our QSO sample. Out of the total of 1000 per GIMIC regions, 727 sightlines were modelled with S/N = 9 per pixel, 182 with S/N = 23 and 91 with S/N = 2. These numbers keep the proportion between the different S/N values as it is in the observed sample (see the last column in Table 1).[8]

We fit Voigt profiles to the synthetic spectra automatically using VPFIT,[9] following the algorithm described by Crighton et al. (2010). First, an initial guess of several absorption lines is generated in each spectrum to minimize χ^2_{reduced}. If the χ^2_{reduced} is greater than a given threshold of 1.1, another absorption component is added at the pixel of largest deviation and χ^2_{reduced} is reminimized. Absorption components are removed if both $N_{\text{HI}} < 10^{14.3}\,\text{cm}^{-2}$ and $b_{\text{HI}} < 0.4\,\text{km s}^{-1}$. This iteration continues until $\chi^2_{\text{reduced}} \leq 1.1$. Then, the Voigt fits are stored. We only kept absorption lines where the values of $\log N_{\text{HI}}$ and b_{HI} are at least five times their uncertainties as quoted by VPFIT.

The fraction of hydrogen in the form of H I within GIMIC is obtained from CLOUDY (Ferland et al. 1998) after assuming an ionization background from Haardt & Madau (1996) that yields a photoionization rate of $\Gamma = 8.59 \times 10^{-14}\,\text{s}^{-1}$. This ionization background is not well constrained at $z \approx 0$, so we use a post-processing correction to account for this uncertainty. In the optically thin regime $\Gamma^{\text{thin}} \propto 1/\tau$, where τ is the optical depth (Gunn & Peterson 1965). Then, scaling the optical depth values is equivalent to scaling the ionization background (e.g. Theuns, Leonard & Efstathiou 1998a; Davé et al. 1999). First, we combined the five GIMIC regions using different volume weights, namely (1/12,

---

[6] Written by Joop Schaye, Craig M. Booth and Tom Theuns.

[7] Note that the majority of the Lyα used in this work were observed with STIS/*HST* rather than *FUSE*.

[8] Note that we have divided the mean S/N per 2-pixel resolution element by $\sqrt{2}$ to have an estimation per pixel.

[9] Written by R. F. Carswell and J. K. Webb (see http://www.ast.cam.ac.uk/~rfc/vpfit.html).

---

[5] Note that GIMIC adopted an $H_0 = 100\,h\,\text{km s}^{-1}\text{Mpc}^{-1}$, $h = 0.73$, $\Omega_m = 0.25$, $\Omega_\Lambda = 0.75$, $\sigma_8 = 0.9$, $k = 0$ cosmology. These parameters are slightly different from the ones used in P12.

Table 3. KS test probabilities between different samples.[a]

	Void/edge (per cent)	Void/uncl. (per cent)	Edge/uncl. (per cent)	Void/not-void (per cent)	Edge/not-edge (per cent)	Uncl./not-uncl. (per cent)
KS-Prob(log $N_{H I}$)	2 (0.7)	74 (66)	56 (24)	4 (4)	3 (0.6)	64 (54)
KS-Prob($b_{H I}$)	8 (6)	18 (17)	71 (75)	7 (7)	20 (14)	32 (32)

[a] Results are presented in a X (D) format (see Section 3.1).
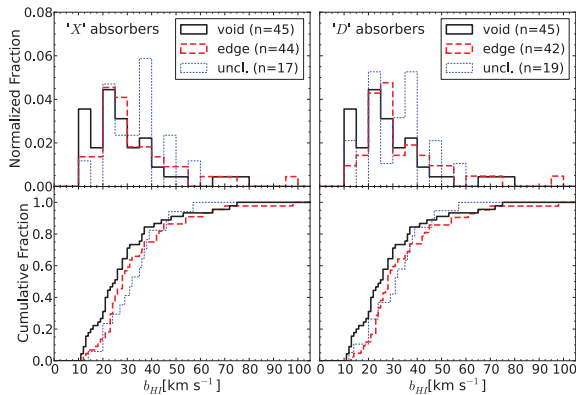
Figure 4. H I Doppler parameter distribution for the three different LSS samples defined in this work (see Section 3.2): void absorbers (black solid lines), void-edge absorbers (red dashed lines) and unclassified absorbers (blue dotted lines). The top panels show the normalized distribution using arbitrary binning of 5 km s^{-1}. The bottom panels show the cumulative distributions for the unbinned samples. The left- and right-hand panels correspond to absorbers defined using the X and D coordinates, respectively.

1/6, 1/2, 1/6, 1/12) for the $(-2, -1, 0, +1, +2)\sigma$ regions, respectively (see appendix 2 in Crain et al. 2009 for a justification of these weights). Then, we searched for a constant value to scale all the original optical depth values such that the mean flux of the combined sample is equal to the observed mean flux of Lyα absorption at low redshift. A second possibility is to scale the optical depth values in order to match the redshift number density of H I lines in some column density range, dN/dz, instead of the mean flux. Ideally, by matching one observable the second would also be matched.

Extrapolating the double power-law fit result from Kirkman et al. (2007) to $z = 0$ (see their equation 6), the observed mean flux is $\langle F \rangle = 0.987$ with a typical statistical uncertainty of $\sigma_{\langle F \rangle} \sim 0.003$. In order to match this number in the simulation, a scale of 1.16 is required in the original optical depth values (0.86 in Γ). From this correction, the redshift number density of lines in the range $10^{13.2} \leq N_{H I} \leq 10^{14}$ cm^{-2} is found to be dN/d$z \approx 50$. For reference, Lehner et al. (2007) and DS08 found dN/d$z \sim 50-90$ over the same column density range. We have repeated the experiment for consistency, using $\langle F \rangle = \{0.984, 0.990\}$ which are within $\pm 1\sigma_{\langle F \rangle}$ of the extrapolated value. To match these, scales of 1.50 and 0.84 are required in the original optical depth values, respectively (0.67 and 1.19 in Γ). From those mean fluxes we found dN/d$z \approx \{70, 35\}$ respectively, along the same column density range. Therefore, a value of $\langle F \rangle = 0.990$ underpredicts the number of H I lines. On the other hand, values of $\langle F \rangle = 0.987$ and 0.984 are in good agreement with observations. In the following analysis, we use $\langle F \rangle = 0.987$ unless otherwise stated.

4.2 Comparison between simulated and observed H I properties
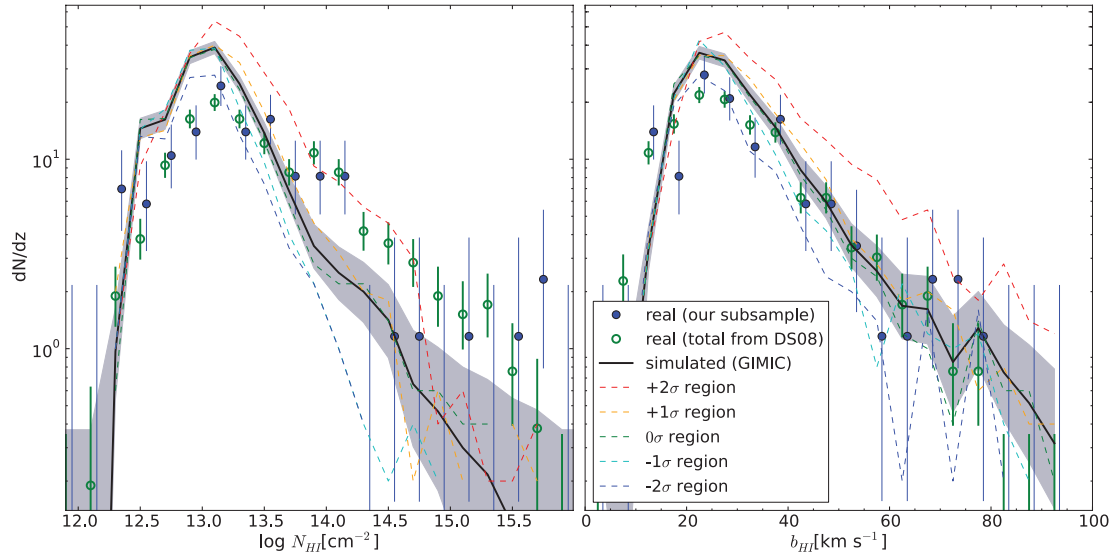
Fig. 5 shows the redshift number density of H I lines (not corrected for incompleteness) as a function of both column density (left-hand panel) and Doppler parameter (right-hand panel). Data from the simulation are shown by the black line (volume-weighted result) and each individual GIMIC region is shown separately by the dashed lines. For comparison, data from observations are also shown. Green open circles correspond to the total sample from DS08 (657 systems), while blue filled circles correspond to the subsample used in this study (106 systems that intersect the SDSS volume). There is not perfect agreement between simulated and real data. We see an excess (lack) of systems with $N_{H I} \lesssim 10^{13.5}$ cm^{-2} ($\gtrsim 10^{14}$ cm^{-2}) in the simulation compared to observations while Doppler parameters are in closer agreement, although there is still a difference at low $b_{H I}$.

Assuming that the column density distribution can be modelled as a power law, the position of the turnover at the low $N_{H I}$ end gives us an estimation of the completeness level of detection in the sample. As the turnover appears to be around $N_{H I} \approx 10^{13}$ cm^{-2} in both simulated and real data (by design), we do not, in principle, attribute the discrepancy in the column density distributions to a wrong choice of the simulated S/N. Raising the mean flux to a greater value than $\langle F \rangle = 0.987$ (less absorption) does not help as the dN/dz in the range $10^{13.2} \leq N_{H I} \leq 10^{14}$ cm^{-2} will then be smaller than the observational result (see Section 4.1). We attempted to get a better match by using a mean flux of $\langle F \rangle = 0.984$ (more absorption), motivated to produce a better agreement at higher column densities. In order to agree at low column densities, we had to degrade the sample S/N to be composed of ~ 400, ~ 100 and ~ 500 sightlines at S/N values of 9, 23 and 2, respectively. It is implausible that half of the observed redshift path has such a poor quality.

Another possibility to explain the discrepancy could be the fact that weak systems in observations were preferentially characterized with the AOD method, whereas here we have only used Voigt profile fitting. In order to test this hypothesis, we have merged closely separated systems (within 150 km s^{-1}) whose summed column density is less than $10^{13.5}$ cm^{-2}. Using these constraints, 43 out of 4179 systems were merged (≈ 1 per cent). Such a small fraction does not have an appreciable effect on the discrepancy. As an extreme case, we have repeated the experiment merging *all* systems within 300 km s^{-1} independently of their column densities. From this, 555 out of 4179 systems were merged (≈ 13 per cent) but still it was not enough to fully correct the discrepancy. Given that the discrepancy is not explained by a systematic effect from different line characterization methods, we chose to keep our original simulated sample in the following analysis without merging any systems.

There is a reported systematic effect by which column densities inferred from a single Lyα line are typically (with large scatter) underestimated with respect to the COG solution. Similarly $b_{H I}$ are typically overestimated (Shull et al. 2000; Danforth et al. 2006;

Figure 5. Redshift number density of H I lines as a function of both column density (left-hand panel) and Doppler parameter (right-hand panel) using arbitrary binning of $\Delta \log N_{\mathrm{HI}} = 0.2$ dex and $\Delta b_{\mathrm{HI}} = 5 \, \mathrm{km \, s^{-1}}$, respectively. Both results have not been corrected for incompleteness. Green open circles correspond to real data from the total sample of DS08 (657 systems), while blue filled circles (slightly offset in the *x*-axes for clarity) correspond to the subsample used in this study (106 systems). The black line corresponds to the volume-weighted result from the combination of the five GIMIC regions where the shaded region corresponds to the $\pm 1\sigma$ uncertainty. Dashed lines show the results from each individual GIMIC region. Error bars correspond to the Poissonian uncertainty from the analytical approximation $\sigma_n^+ \approx \sqrt{n + 3/4} + 1$ and $\sigma_n^- \approx \sqrt{n - 1/4}$ (Gehrels 1986).

see also Section A2 for discussion on how this may affect our observational results). This effect is only appreciable for $N_{\mathrm{HI}} \gtrsim 10^{14} \, \mathrm{cm}^{-2}$ and is bigger for saturated lines. Given that our simulated sample was constructed to reproduce the observed sample, this effect could be present. If so, it would, in principle, help to reduce the discrepancy at the high column density end. From fig. 3 of Danforth et al. (2006), we have inferred a correction for systems with $N_{\mathrm{HI}} \geq 10^{13.5} \, \mathrm{cm}^{-2}$ of

$$\log N_{\mathrm{HI}}^{\mathrm{corr}} = \frac{\log N_{\mathrm{HI}}^{\mathrm{obs}} - 8.37}{1 - 0.62}, \tag{3}$$

where $N_{\mathrm{HI}}^{\mathrm{corr}}$ and $N_{\mathrm{HI}}^{\mathrm{obs}}$ are the corrected and observed N_{HI} values, respectively. From this correction, we found an increase in the number of systems at $N_{\mathrm{HI}} \gtrsim 10^{14.5} \, \mathrm{cm}^{-2}$ up to values consistent with observations. This, however, does not help with the discrepancy at lower column densities.

At this point, it is difficult to reconcile the simulation result with the real data using only a single effect. We note that the discrepancy is a factor of ~ 2 only, so it could be in principle explained through a combination of several observational effects. Also note that the number of observed lines at higher column densities is still small and it could be affected by low number statistics. The lack of systems with very low N_{HI} and b_{HI} values can be explained by our selection of the highest S/N value of 23, while in real data there could be regions with higher values. It is not the aim of this section to have a perfect match between simulations and observations, but rather examine the qualitative differences between simulated regions of different densities. Thus, hereafter, we will use the results from the simulation in its original form (as shown in Fig. 5), i.e. without any of the aforementioned corrections.

### 4.3 Simulated H I absorbers' properties in different LSS regions

Given that GIMIC does not provide enough volume to perform a completely analogous search for voids (each region is $\sim 20 \, h^{-1}$ Mpc

of radius), we use them only as crude guides to compare our results with. We could consider the -2σ region as representative of void regions as it is actually centred in one. Naively, we could consider the 0σ regions as representative of void-edge regions, as it is there where the mean cosmological density is reached. A direct association for the $+1\sigma$ and $+2\sigma$ is not so simple though, as they would be associated with some portions of the void-edge regions too. It seems more reasonable to use the GIMIC spheres as representative of different density environments then, where $-2\sigma/+2\sigma$ correspond to extremely underdense/overdense regions and so on. For reference, the whole $(-2, -1, 0, +1, +2)\sigma$ GIMIC regions correspond to densities of $\rho/\langle\rho\rangle \approx (0.4, 0.6, 0.9, 1.2, 1.8)^{10}$ at $z = 0$, respectively, where $\langle\rho\rangle$ is the mean density of the Universe (see fig. A1 from Crain et al. 2009).

Fig. 6 shows the cumulative distributions of N_{HI} (left-hand panel) and b_{HI} (right-hand panel). Results from each of the individual GIMIC region are shown by dashed lines. Void and void-edge absorbers are shown by solid black and red lines, respectively. For simplicity, we show only LSS definition based on X. Cumulative distributions between real and simulated data do not agree perfectly. However, in both real and simulated data, there is an offset between column densities and Doppler parameters found in different environments. Low-density environments have smaller values for both N_{HI} and b_{HI} than higher density ones (and vice versa). This trend still holds when using an S/N = 23 per pixel for the 5000 sightlines.

The KS test gives a significant difference between the $+2\sigma$, $+1\sigma$ and $+0\sigma$ regions, and any other GIMIC region at the $\gg 99$ per cent, $\gtrsim 99$ per cent and $\gtrsim 95$ per cent c.l., respectively, in both N_{HI} and b_{HI} distributions. The KS test gives no significant difference between the -2σ and -1σ regions in both N_{HI} and b_{HI} distributions (see Table 4). These results do not change significantly when correcting GIMIC to match the observed N_{HI} distribution

---

[10] Given that we are using cubic subvolumes centred in these spheres, these cubes should have higher density differences between them.
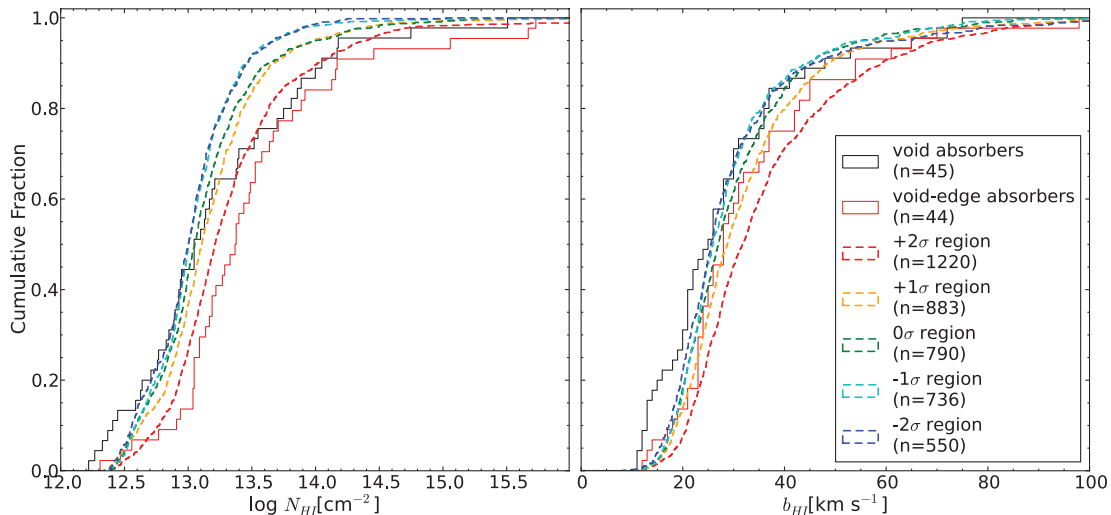
Figure 6. Column density (left-hand panel) and Doppler parameter (right-hand panel) cumulative distributions for H I. Void absorbers are shown by solid black lines, while void-edge absorbers are shown by solid red lines. Dashed lines show the result from each individual GIMIC region. For simplicity, we only show LSS definitions based on X.

Table 4. KS test probabilities between different GIMIC regions.[a]

$N_{\rm HI}/b_{\rm HI}$	-2σ	-1σ	0σ	$+1\sigma$	$+2\sigma$
-2σ	...	30%	2%	2%	≪1%
-1σ	77%	...	6%	≪1%	≪1%
0σ	11%	0.9%	...	0.7%	≪1%
$+1\sigma$	≪1%	≪1%	0.4%	...	≪1%
$+2\sigma$	≪1%	≪1%	≪1%	≪1%	...

[a] KS test probabilities (percentage values) for $\log N_{\rm HI}$ and $b_{\rm HI}$ distributions are shown in the left-bottom and right-upper sides, respectively. ≪1 per cent corresponds to values $<10^{-4}$ per cent.

using a different $\langle F \rangle$ and S/N values. We do not attempt to make a more detailed comparison between distributions coming from real data (void, void-edge samples) and the different GIMIC regions as there are already known differences between them (see Section 4.2).

5 DISCUSSION

5.1 Three Lyα forest populations

Our first result is that there is a >99 per cent c.l. excess of Lyα systems at the edges of galaxy voids compared to a random distribution (see Section 3.1 and Fig. 1). Our random sample was normalized to have the same density of systems in the whole volume. Then, an excess in a subvolume means necessarily a deficit in another. Given that we found no significant difference in the number of systems in voids with respect to the random expectation, the excess is not explained by a deficit of Lyα systems inside galaxy voids. The observed excess seems more related to the lack of systems found at distances $\gtrsim 5\,h^{-1}$ Mpc outside the catalogued voids (and vice versa). Thus, despite the fact that we see Lyα clustered at the edges of galaxy voids, it is not clear from these data that Lyα voids at low z exist at all (see Carswell & Rees 1987 for similar result at high z; although see Williger et al. 2000). This picture is somewhat different from the case of galaxies, where galaxy voids are present

even in the distribution of low-mass galaxies (e.g. Peebles 2001; Tikhonov & Klypin 2009). There is agreement though in the sense that both Lyα system and galaxy distributions have their peaks at the edges of galaxy voids. We observe a typical scale length of the excess to be $\sim 5\,h^{-1}$ Mpc, consistent with numerical predictions for the typical radius of the filamentary structure of the 'cosmic web' ($\sim 2\,h^{-1}$ Mpc; see Aragón-Calvo et al. 2010; Bond et al. 2010; González & Padilla 2010). Note that this scale length is approximately twice the scale associated with a velocity uncertainty of $\Delta v \approx 200\,\mathrm{km\,s^{-1}}$ at $z = 0$. Such dispersions could be present in our void-edge sample.

In our data analysis we have defined three samples of absorption systems, based on how they are located with respect to the closest galaxy void (see Section 3.2). Let us consider now a very simple model in which we have only two LSS environments: underdense and overdense LSS. Then we could relate all the 'random-like' Lyα forest systems found in the void sample ($X < 0.9$ and/or $D < -2\,h^{-1}$ Mpc) with the underdense LSS, while all the systems associated with the excess over random ($0.9 \leq X < 1.3$ and/or $-2 \leq D < 4\,h^{-1}$ Mpc) to the overdense LSS.[11] Note that the fact that we cannot distinguish between the underdense LSS Lyα distribution and a random distribution does not mean that the former is really random. If these Lyα forest systems follow the underlying dark matter distribution (e.g. see Croft et al. 1998), they should have a non-negligible clustering amplitude that is not observed only because of the lack of statistical power of our sample. In relative terms, considering the underdense LSS Lyα as random seems to be a good approximation though, especially for the large-scale distances involved in this work (>1 Mpc). This is also supported by the very low autocorrelation amplitude observed in the whole population of Lyα forest systems at such scales (e.g. Croft et al. 1998; Rollinde et al. 2003; Crighton et al. 2011). This 'random' behaviour of Lyα systems in the underdense LSS can be understood as originating in structures still evolving from the primordial density perturbations in the linear regime. However, at $z = 0$ the majority of the mass resides at the edges of voids (in the 'cosmic web') whose density perturbations have reached non-linear evolution regime at higher

---

[11] We have left the unclassified systems out of this interpretation.

redshifts. For reference, we expect the underdense and overdense LSS to have typical $\delta \gtrsim 0$ and $\delta \lesssim 0$ respectively, where δ is the density contrast defined as

$$\delta \equiv \frac{\rho - \langle \rho \rangle}{\langle \rho \rangle}, \tag{4}$$

where ρ is the density and $\langle \rho \rangle$ is the mean density of the Universe. Note, however, that these LSS environments are not defined by a particular density but rather by a topology (voids, walls, filaments).

Theoretical arguments point out that the observed column density of neutral hydrogen at a fixed z is

$$N_{\mathrm{HI}} \propto \rho_{\mathrm{H}}^{1.5} \, T^{-0.26} \, \Gamma^{-1} \, f_{\mathrm{g}}^{0.5}, \tag{5}$$

where ρ_{H} is the density of hydrogen, T is the temperature of the gas, Γ is the hydrogen photoionization rate and f_{g} is the fraction of mass in gas (Schaye 2001). In the diffuse IGM it has been predicted that $T \propto \rho_{\mathrm{H}}^{\alpha}$, where $\alpha \approx 0.59$ (Hui & Gnedin 1997). This implies that for a fixed Γ, the main dependence of N_{HI} is due to ρ_{H} as $N_{\mathrm{HI}} \propto \rho_{\mathrm{H}}^{1.4}$. Then, despite the extremely low densities inside galaxy voids we can still observe Lyα systems, although only the ones corresponding to the densest structures.

Let us consider the predicted ratio between N_{HI} observed inside voids and at the edges of voids as

$$\frac{N_{\mathrm{HI}}^{\mathrm{void}}}{N_{\mathrm{HI}}^{\mathrm{edge}}} \approx \left(\frac{\rho_{\mathrm{H}}^{\mathrm{void}}}{\rho_{\mathrm{H}}^{\mathrm{edge}}} \right)^{1.4} \left(\frac{\Gamma^{\mathrm{void}}}{\Gamma^{\mathrm{edge}}} \right)^{-1} \left(\frac{f_{\mathrm{g}}^{\mathrm{void}}}{f_{\mathrm{g}}^{\mathrm{edge}}} \right)^{0.5}. \tag{6}$$

Given that the time-scale for photons to travel along ~ 10–$20 \, h^{-1}$ Mpc is $\ll 1$ Gyr, we can consider $\Gamma^{\mathrm{void}} \approx \Gamma^{\mathrm{edge}}$. Even if we assume that the gas inside voids has not formed galaxies, $f_{\mathrm{g}}^{\mathrm{void}} \gtrsim f_{\mathrm{g}}^{\mathrm{edge}}$, because f_{g} is dominated by the dark matter. This implies that a given observed N_{HI} inside and at the edge of galaxy voids will correspond to similar densities of hydrogen ($\rho_{\mathrm{H}}^{\mathrm{void}} \approx \rho_{\mathrm{H}}^{\mathrm{edge}}$). This is important because it means that the Lyα forest in the underdense LSS is not different from the overdense LSS one, and two systems with equal N_{HI} are comparable, independently of its large-scale environment.

If there were no galaxies, this simple model may suffice to explain the differences in the observed Lyα population. The fact that some of the Lyα systems are directly associated with galaxies cannot be neglected though. There is strong evidence from observations (e.g. Lanzetta et al. 1995; Chen et al. 1998; Morris & Jannuzi 2006; Stocke et al. 2006; Chen & Mulchaey 2009; Crighton et al. 2011; Prochaska et al. 2011; Rakic et al. 2012; Rudie et al. 2012) and simulations (e.g. Fumagalli et al. 2011; Stinson et al. 2011) that $N_{\mathrm{HI}} \gtrsim 10^{15}$ cm^{-2} systems are preferentially found within a couple of hundred kpc of galaxies. Probably an appropriate interpretation of such a result is that galaxies are always found in 'local' ($\lesssim 100 \, h^{-1}$ kpc) high density regions. Then, a plausible scenario would require *at least* three types of Lyα forest systems: (1) containing embedded galaxies, (2) associated with overdense LSS but with no close galaxy and (3) associated with underdense LSS but with no close galaxy. For convenience, we will refer to the first type as 'halo-like', although with the caution that these systems may not be gravitationally bound with the galaxy.

Given that there are galaxies inside galaxy voids, the 'halo-like' Lyα systems will be present in both low- and high-density LSS environments (galaxies are a 'local' phenomenon). The contribution of the 'halo-like' in galaxy voids could be considered small though. Assuming this contribution to be negligible, we can estimate the fraction of Lyα systems in the underdense LSS as ≈ 25–30 ± 6 per

cent.[12] Likewise, ≈ 70–75 ± 12 per cent of the Lyα forest population is due to a combination of systems associated with galaxies and with the overdense LSS. We could estimate the contribution of 'halo-like' absorbers by directly looking for and counting galaxies relatively close to the absorption systems. A rough estimation can be done by assuming that galaxy haloes will have only $N_{\mathrm{HI}} \geq 10^{14}$ cm^{-2} systems, leading to a contribution of ≈ 12–15 ± 4 per cent[13] in our sample.

In summary, our results require *at least* three types of Lyα systems to explain the observed Lyα forest population at low-z ($N_{\mathrm{HI}} \gtrsim 10^{12.5}$ cm^{-2}).

(i) *Halo-like*: Lyα with embedded nearby galaxies ($\lesssim 100 \, h^{-1}$ kpc) and so directly correlated with galaxies (≈ 12–15 ± 4 per cent).

(ii) *Overdense LSS*: Lyα associated with the overdense LSS that are correlated with galaxies only because both populations lie in the same LSS regions (≈ 50–55 ± 13 per cent).

(iii) *Underdense LSS*: Lyα associated with the underdense LSS with very low autocorrelation amplitude that are not correlated with galaxies (≈ 25–30 ± 6 per cent).

The relative contribution of these different Lyα populations is a function of the lower N_{HI} limit. Low N_{HI} systems dominate the Lyα column density distribution. Then, given that underdense LSS Lyα systems tend to be of lower column density than the other two types, we expect the contribution of 'random-like' Lyα to increase (decrease) while observing at lower (higher) N_{HI} limits. Note that there are not sharp N_{HI} limits to differentiate between our three populations (see Fig. 2). The 'halo-like' is defined by being close to galaxies, while the 'LSS-like' ones are defined in terms of an LSS topology (voids, wall, filaments).

Motivated by a recently published study on the Lyα/galaxy association by Prochaska et al. (2011), we can set a conservative upper limit to the 'halo-like' contribution. These authors have found that nearly all their observed $L \geq 0.01L^*$ galaxies (33/37) have $N_{\mathrm{HI}} \geq 10^{13.5}$ cm^{-2} absorption at impact parameters $< 300 \, h_{72}^{-1}$ kpc. If we invert the reasoning and assume an extreme (likely unrealistic) scenario where *all* the $N_{\mathrm{HI}} \geq 10^{13.5}$ cm^{-2} are directly associated with galaxies, then the 'halo-like' contribution will have an upper limit of $< 33 \pm 7$ per cent.[14] Consequently, the contribution of the overdense LSS to the Lyα population will be > 37–42 ± 14 per cent. Still, note that we have found several systems with $10^{13.5} \lesssim N_{\mathrm{HI}} \lesssim 10^{14.5}$ cm^{-2} inside galaxy voids for which a direct association with galaxies is dubious (see Fig. 2). Also note that only ~ 10 per cent (~ 0 per cent) of the Lyα systems in the range of $10^{13.5} < N_{\mathrm{HI}} < 10^{14.5}$ cm^{-2} may be associated with a galaxy at impact parameters < 300 kpc (< 100 kpc) in the Prochaska et al. (2011) sample (see their fig. 4).

Our findings are consistent with previous studies pointing out a non-negligible contribution of 'random' Lyα systems (at a similar N_{HI} limit) of ≈ 20–30 per cent (Mo & Morris 1994; Stocke et al. 1995; Penton et al. 2002). These authors estimated that ≈ 70–80 per cent of the Lyα population is associated with either LSS (galaxy

---

[12] These numbers come from $28 \pm 5 \, (22 \pm 5)$ and $61 \pm 8 \, (65 \pm 8)$ systems found at $X < 0.9 \, (D < -2 \, h^{-1}$ Mpc) and at $0.9 \leq X < 1.3 \, (-2 \leq D < 4 \, h^{-1}$ Mpc), respectively (see Section 3.1).

[13] From either 13/89 (excluding the unclassified sample) or 13/106 (including the unclassified sample). We have assumed Poisson uncertainty.

[14] From either 29/89 (excluding the unclassified sample) or 35/106 systems in our sample (including the unclassified sample). We have assumed Poisson uncertainty.

filaments) or galaxies. Note that Mo & Morris (1994) put an upper limit of ≈20 per cent being directly associated with galaxies, which is also consistent with our estimation. Our result is also in accordance with the previous estimation that 22 ± 8 per cent (Penton et al. 2002; based on eight systems) and 17 ± 4 per cent (Wakker & Savage 2009; based on 17 systems) of the Lyα systems lie in voids (defined as locations at $>3\,h_{70}^{-1}$ Mpc from the closest $>L^*$ galaxy). This is in contrast with early models that associated *all* Lyα systems with galaxies (e.g. Lanzetta et al. 1995; Chen et al. 1998).

Although there is general agreement with recently proposed models to explain the origin of the low-z Lyα forest (e.g. Wakker & Savage 2009; Prochaska et al. 2011), we emphasize that our interpretation is qualitatively different and adds an important component to the picture: the presence of the underdense LSS ('random-like') systems. For instance, assuming infinite filaments of typical widths of ≈400 h_{72}^{-1} kpc around galaxies, Prochaska et al. (2011) argued that *all* Lyα systems at low z belong either to the circumgalactic medium (CGM;[15] which includes our 'galaxy halo' definition) or the filamentary structure in which galaxies reside (equivalent to our overdense LSS definition). Our findings are not fully consistent with this hypothesis, as neither the 'CGM model' nor the 'galaxy filament model' seem likely to explain the majority of our underdense LSS absorbers at $N_{\rm HI} \lesssim 10^{13.5}$ cm^{-2}. To do so there would need to be a whole population of unobserved galaxies (dwarf spheroidals?) inside galaxy voids with an autocorrelation amplitude as low as the 'random-like' Lyα one. As discussed by Tikhonov & Klypin (2009), very low surface brightness dwarf spheroidals could be a more likely explanation than dwarf irregulars because the latter should have been observed with higher incidences in recent H I emission blind surveys inside galaxy voids (e.g. Doyle et al. 2005). On the other hand, the formation of dwarf spheroidals inside galaxy voids is difficult to be explained from the current galaxy formation paradigm (see Tikhonov & Klypin 2009 for further discussion). As mentioned, it seems more natural to relate the majority of the underdense LSS absorbers with the peaks of extremely low-density structures inside galaxy voids, still evolving linearly from the primordial density perturbations that have not yet formed galaxies because of their low densities. Our interpretation can be tested by searching for galaxies close to our lowest $N_{\rm HI}$ void absorbers (see Fig. 2). Another prediction of our interpretation is that the vast majority of $N_{\rm HI} \lesssim 10^{13}$ cm^{-2} systems should reside inside galaxy voids. If the QSO sightlines used here were observed at higher sensitivities, weak Lyα systems should preferentially appear at $X < 1$ ($D < 0\,h^{-1}$ Mpc). Therefore, we should expect to have an anticorrelation between $N_{\rm HI} \lesssim 10^{13}$ cm^{-2} and galaxies.

5.2 $N_{\rm HI}$ and $b_{\rm HI}$ distributions

Our second result is that there is a systematic difference ($\gtrsim 98$ per cent c.l.) between the column density distributions of Lyα systems found within, and those found at the edge of, galaxy voids. Void absorbers have more low column density systems than the void-edge sample (see Fig. 3). A similar trend is found in GIMIC, where

---

[15] According to the Prochaska et al. (2011) definition 'the CGM corresponds to highly ionized medium around galaxies at distances greater than the virial radius but smaller than ~300 kpc that need not be causally connected (associated, gravitationally bound) with these galaxies'. We do not see a clear advantage of adopting this terminology and so we use 'IGM' instead to refer to the same medium. We only make a distinction between LSS (voids, walls, filaments) and the ones with embedded nearby galaxies ($\lesssim 100\,h^{-1}$ kpc).

low-density environments present smaller $N_{\rm HI}$ values than higher density ones (see Fig. 6, left-hand panel). This can be explained by the fact that baryonic matter follows the underlying dark matter distribution. Then, the highest density environments should be located at the edges of voids (in the intersection of walls and filaments), consequently producing higher column density absorption than in galaxy voids (e.g. see Schaye 2001).

Also, by construction, there is a higher chance to find galaxies at the edges rather than inside galaxy voids. Assuming that some of the Lyα forest systems are associated with galaxy haloes (see Section 5.1 for further discussion), this population should be present mainly in our void-edge sample. As galaxy haloes correspond to local density peaks, we should also expect on average higher column density systems in this population. Given that galaxies may affect the properties of the surrounding gas, there could be processes that only affect Lyα systems close to galaxies. For instance, the distribution of Lyα systems around galaxy voids seems to show a two-peaked shape (see Fig. 1). We speculate that this could be a signature of neutral hydrogen being ionized by the UV background produced by galaxies (see also Adelberger et al. 2003), mostly affecting $N_{\rm HI} \lesssim 10^{13}$ cm^{-2} inside the filamentary structure of the 'cosmic web'. Another explanation could be that in the inner parts of the filamentary structure, Lyα systems get shock heated by the large gravitational potentials, raising their temperature and ionization state (e.g. Cen & Ostriker 1999). A third possibility is that it could be a signature of bulk outflows as the shift between peaks is consistent with a $\Delta v \approx 200$–300 km s^{-1}. On the other hand, the two peaks could have distinct origins as the first one may be related to an excess of $N_{\rm HI} \lesssim 10^{13}$ cm^{-2} systems, probably associated with the overdense LSS in which galaxies reside, while the second one may be related to an excess of $N_{\rm HI} \gtrsim 10^{14}$ cm^{-2} systems, more likely associated with systems having embedded galaxies. As mentioned, we cannot prove the reality of this two-peaked signature at a high confidence level from the current sample and so we leave the confirmation or disproof of these hypotheses to future studies.

The GIMIC data analysis shows a clear differentiation of $b_{\rm HI}$ distributions in different density environments (see Fig. 6, right-hand panel). Low-density environments have smaller $b_{\rm HI}$ values than higher density ones. We see a similar trend in the real data between our void and void-edge absorber samples, although only at a $\gtrsim 90$ per cent c.l. (i.e. not very significant; see Fig. 4). The main mechanisms that contribute to the observed line broadening are temperature, local turbulence and bulk motions of the gas (excluding systematic effects from the line fitting process or degeneracy with $N_{\rm HI}$ for saturated lines). Naturally, in high-density environments, we would expect to have greater contributions from both local turbulence and bulk motions compared to low-density ones. The gas temperature is also expected to increase from low-density environments to high-density ones. As previously mentioned, theoretical arguments predict that the majority of the diffuse IGM will have temperatures related to the density by $T \propto \rho^\alpha$ with $\alpha > 0$ (Hui & Gnedin 1997; Theuns et al. 1998b; Schaye et al. 1999). This is also seen in density–temperature diagrams drawn from current hydrodynamical cosmological simulations (e.g. Davé et al. 2010; Tepper-García et al. 2012). Therefore, our findings are consistent with current expectations.

5.3 Future work

The high sensitivity of the recently installed Cosmic Origins Spectrograph (COS/*HST*; Green et al. 2012) in the UV (especially the

far-UV) will allow us to improve the N_{HI} completeness limit compared with current surveys. This will considerably increase the number of observed Lyα absorption systems at low-z. In the short term, there are several new QSO sightlines scheduled for observations (or already observed) with COS/*HST* that intersect the SDSS volume. Combining these with current and future galaxy void catalogues, we expect to increase the statistical significance of the results presented in this work. COS/*HST* will also allow observations of considerably more metal lines (especially O VI) than current IGM surveys. Again, in combination with LSS surveys, this will be very useful for studies on metal enrichment in different environments. For instance, we have identified eight systems with observed O VI absorption from STIS/*HST* in our sample. Three of these lie inside voids at $X \approx \{0.6, 0.7, 0.9\}$ ($D \approx \{-5.4, -4.6, -1.6\}\,h^{-1}$ Mpc), respectively. The first two systems that lie inside voids correspond to the highest N_{HI} values ($N_{\mathrm{HI}} > 10^{14.5}$ cm^{-2}; see Fig. 2). We have performed a search in the SDSS DR8 for galaxies in a cylinder of radius $1\,h_{71}^{-1}$ Mpc and within ± 200 km s^{-1} around these two absorbers (both systems belong to the same sightline and are at a similar redshift; one of them shows C IV absorption also). We found nine galaxies with these constraints, hinting on a possible association of these systems with a void galaxy. The one at the very edge of the void limit has $N_{\mathrm{HI}} = 10^{13.14 \pm 0.07}$ cm^{-2} and $N_{\mathrm{O\,VI}} = 10^{13.69 \pm 0.18}$ cm^{-2}, and it could in principle be associated with the overdense LSS. The other five O VI absorbers lie in our void-edge sample and have $N_{\mathrm{HI}} > 10^{13.5}$ cm^{-2}, so they are likely to be associated with galaxies. None of the observed O VI lie in our unclassified sample. The current sample of O VI systems is very small, and so we do not aim to draw statistical conclusions from them. However, these systems individually offer interesting cases worth further investigation. We intend to perform a careful search for galaxies that could be associated with each of the Lyα absorbers presented in our sample in future work. In the longer term, it will be possible to extend similar analysis to well-defined galaxy filaments and clusters when the new generation of galaxy surveys are released.

A scenario with three different types of Lyα forest systems, as proposed here, can help to interpret recent measurements of the cross-correlation between Lyα and galaxies (Chen et al. 2005; Ryan-Weber 2006; Wilman et al. 2007; Chen & Mulchaey 2009; Shone et al. 2010; Rudie et al. 2012). These studies come mainly from pencil beam galaxy surveys around QSO sightlines where identifying LSS such as voids or filaments is more challenging. As mentioned, different Lyα systems are not separated by well-defined N_{HI} limits and so we suggest using our results to properly account for underdense LSS ('random-like') absorbers in gas/galaxy cross-correlations. Truly random distributions are easy to correct for, as they lower the amplitude of the correlations at all scales. Then, acknowledging these 'random-like' absorbers, it will be possible to split the correlation power in its other two main components: gas in galaxy haloes and gas in the overdense LSS. Our group is currently working in a future paper to study the gas/galaxy cross-correlation, in which these corrections will be taken into account.

6 SUMMARY

We have presented a statistical study of H I Lyα absorption systems found within and around galaxy voids at $z \lesssim 0.1$. We found a significant excess (>99 per cent c.l.) of Lyα systems at the edges of galaxy voids with respect to a random distribution, over a $\sim 5\,h^{-1}$ Mpc scale. We have interpreted this excess as being due to Lyα systems associated with both galaxies ('halo-like') and the overdense LSS

where galaxies reside (the observed 'cosmic web'), accounting for ≈ 70–75 ± 12 per cent of the Lyα population. We found no significant difference in the number of systems inside galaxy voids compared to the random expectation. We therefore infer the presence of a third type of Lyα systems associated with the underdense LSS with a low autocorrelation amplitude ($\approx$random) that are not associated with luminous galaxies. These 'random-like' absorbers are mainly found in galaxy voids. We argue that these systems can be associated with structures still growing linearly from the primordial density fluctuations at $z = 0$ that have not yet formed galaxies because of their low densities. Although the presence of a 'random' population of Lyα absorbers was also inferred (or assumed) in previous studies, our work presents for the first time a simple model to explain it (see Section 5.1). Above a limit of $N_{\mathrm{HI}} \gtrsim 10^{12.5}$ cm^{-2}, we estimate that ≈ 25–30 ± 6 per cent of Lyα forest systems are 'random-like' and not correlated with luminous galaxies. Assuming that *only* $N_{\mathrm{HI}} \geq 10^{14}$ cm^{-2} systems have embedded galaxies nearby, we have estimated the contribution of the 'halo-like' Lyα population to be ≈ 12–15 ± 4 per cent and consequently ≈ 50–55 ± 13 per cent of the Lyα systems to be associated with the overdense LSS.

We have reported differences between both the column density (N_{HI}) and the Doppler parameter (b_{HI}) distributions of Lyα systems found inside and at the edge of galaxy voids observed at the >98 per cent and >90 per cent c.l., respectively. Low-density environments (voids) have smaller values for both N_{HI} and b_{HI} than higher density ones (edges of voids). These trends are theoretically expected. We have performed a similar analysis using simulated data from GIMIC, a state-of-the-art hydrodynamical cosmological simulation. Although GIMIC did not give a perfect match to the observed column density distribution, the aforementioned trends were also seen. Any discrepancy between GIMIC and real data could be due to low number statistic fluctuations and/or a combination of several observational effects.

In summary, our results are consistent with the expectation that the mechanisms shaping the properties of the Lyα forest are different in different LSS environments. By focusing on a 'large-scale' ($\gtrsim 10$ Mpc) point of view, our results offer a good complement to previous studies on the IGM/galaxy connection based on 'local' scales ($\lesssim 2$ Mpc).

REFERENCES

Abazajian K. N. et al., 2009, ApJS, 182, 543
Adelberger K. L., Steidel C. C., Shapley A. E., Pettini M., 2003, ApJ, 584, 45
Aragón-Calvo M. A., van de Weygaert R., Jones B. J. T., 2010, MNRAS, 408, 2163
Baugh C. M., Lacey C. G., Frenk C. S., Granato G. L., Silva L., Bressan A., Benson A. J., Cole S., 2005, MNRAS, 356, 1191
Benson A. J., Hoyle F., Torres F., Vogeley M. S., 2003, MNRAS, 340, 160
Bond J. R., Kofman L., Pogosyan D., 1996, Nat, 380, 603
Bond N. A., Strauss M. A., Cen R., 2010, MNRAS, 409, 156

Borgani S., Governato F., Wadsley J., Menci N., Tozzi P., Quinn T., Stadel J., Lake G., 2002, MNRAS, 336, 409

Bower R. G., Benson A. J., Malbon R., Helly J. C., Frenk C. S., Baugh C. M., Cole S., Lacey C. G., 2006, MNRAS, 370, 645

Carswell R. F., Rees M. J., 1987, MNRAS, 224, 13p

Ceccarelli L., Padilla N. D., Valotto C., Lambas D. G., 2006, MNRAS, 373, 1440

Cen R., Ostriker J. P., 1999, ApJ, 514, 1

Chen H.-W., Mulchaey J. S., 2009, ApJ, 701, 1219

Chen H.-W., Lanzetta K. M., Webb J. K., Barcons X., 1998, ApJ, 498, 77

Chen H.-W., Prochaska J. X., Weiner B. J., Mulchaey J. S., Williger G. M., 2005, ApJ, 629, L25

Colberg J. M., Sheth R. K., Diaferio A., Gao L., Yoshida N., 2005, MNRAS, 360, 216

Colberg J. M. et al., 2008, MNRAS, 387, 933

Colless M. et al., 2001, MNRAS, 328, 1039

Crain R. A. et al., 2009, MNRAS, 399, 1773

Crighton N. H. M., Morris S. L., Bechtold J., Crain R. A., Jannuzi B. T., Shone A., Theuns T., 2010, MNRAS, 402, 1273

Crighton N. H. M. et al., 2011, MNRAS, 414, 28

Croft R. A. C., Weinberg D. H., Katz N., Hernquist L., 1998, ApJ, 495, 44

Dalla Vecchia C., Schaye J., 2008, MNRAS, 387, 1431

Danforth C. W., Shull J. M., 2008, ApJ, 679, 194 (DS08)

Danforth C. W., Shull J. M., Rosenberg J. L., Stocke J. T., 2006, ApJ, 640, 716

Davé R., Hernquist L., Katz N., Weinberg D. H., 1999, ApJ, 511, 521

Davé R., Oppenheimer B. D., Katz N., Kollmeier J. A., Weinberg D. H., 2010, MNRAS, 408, 2051

Doyle M. T. et al., 2005, MNRAS, 361, 34

Ferland G. J., Korista K. T., Verner D. A., Ferguson J. W., Kingdon J. B., Verner E. M., 1998, PASP, 110, 761

Fukugita M., Peebles P. J. E., 2004, ApJ, 616, 643

Fukugita M., Hogan C. J., Peebles P. J. E., 1998, ApJ, 503, 518

Fumagalli M., Prochaska J. X., Kasen D., Dekel A., Ceverino D., Primack J. R., 2011, MNRAS, 418, 1796

Gehrels N., 1986, ApJ, 303, 336

González R. E., Padilla N. D., 2010, MNRAS, 407, 1449

Green J. C. et al., 2012, ApJ, 744, 60

Gunn J. E., Peterson B. A., 1965, ApJ, 142, 1633

Haardt F., Madau P., 1996, ApJ, 461, 20

Hoyle F., Vogeley M. S., 2002, ApJ, 566, 641

Hui L., Gnedin N. Y., 1997, MNRAS, 292, 27

Icke V., 1984, MNRAS, 206, 1p

Kirkman D., Tytler D., Lubin D., Charlton J., 2007, MNRAS, 376, 1227

Kreckel K. et al., 2011, AJ, 141, 4

Lanzetta K. M., Bowen D. V., Tytler D., Webb J. K., 1995, ApJ, 442, 538

Lehner N., Savage B. D., Richter P., Sembach K. R., Tripp T. M., Wakker B. P., 2007, ApJ, 658, 680

Lewis I. et al., 2002, MNRAS, 334, 673

Lopez S. et al., 2008, ApJ, 679, 1144

Mo H. J., Morris S. L., 1994, MNRAS, 269, 52

Moos H. W. et al., 2000, ApJ, 538, L1

Morris S. L., Jannuzi B. T., 2006, MNRAS, 367, 1261

Morris S. L., van den Bergh S., 1994, ApJ, 427, 696

Morris S. L., Weymann R. J., Dressler A., McCarthy P. J., Smith B. A., Terrile R. J., Giovanelli R., Irwin M., 1993, ApJ, 419, 524

Padilla N., Lacerna I., Lopez S., Barrientos L. F., Lira P., Andrews H., Tejos N., 2009, MNRAS, 395, 1135

Padilla N., Lambas D. G., González R., 2010, MNRAS, 409, 936

Pan D. C., Vogeley M. S., Hoyle F., Choi Y.-Y., Park C., 2012, MNRAS, 421, 926 (P12)

Park C., Choi Y.-Y., Vogeley M. S., Gott J. R., III, Blanton M. R., SDSS Collaboration, 2007, ApJ, 658, 898

Peebles P. J. E., 2001, ApJ, 557, 495

Penton S. V., Stocke J. T., Shull J. M., 2002, ApJ, 565, 720

Prochaska J. X., Tumlinson J., 2009, in Thronson H. A., Stiavelli M., Tielens A., eds, Baryons: What, When and Where?. Springer, Netherlands, p. 419

Prochaska J. X., Weiner B., Chen H.-W., Mulchaey J., Cooksey K., 2011, ApJ, 740, 91

Rakic O., Schaye J., Steidel C. C., Rudie G. C., 2012, ApJ, 751, 94

Regos E., Geller M. J., 1991, ApJ, 377, 14

Rojas R. R., Vogeley M. S., Hoyle F., Brinkmann J., 2005, ApJ, 624, 571

Rollinde E., Petitjean P., Pichon C., Colombi S., Aracil B., D'Odorico V., Haehnelt M. G., 2003, MNRAS, 341, 1279

Rudie G. C. et al., 2012, ApJ, 750, 67

Ryan-Weber E. V., 2006, MNRAS, 367, 1251

Savage B. D., Sembach K. R., 1991, ApJ, 379, 245

Schaye J., 2001, ApJ, 559, 507

Schaye J., Dalla Vecchia C., 2008, MNRAS, 383, 1210

Schaye J., Theuns T., Leonard A., Efstathiou G., 1999, MNRAS, 310, 57

Schaye J. et al., 2010, MNRAS, 402, 1536

Sheth R. K., van de Weygaert R., 2004, MNRAS, 350, 517

Shone A. M., Morris S. L., Crighton N., Wilman R. J., 2010, MNRAS, 402, 2520

Shull J. M. et al., 2000, ApJ, 538, L13

Shull J. M., Smith B. D., Danforth C. W., 2011, preprint (arXiv:1112.2706)

Spinrad H. et al., 1993, AJ, 106, 1

Springel V. et al., 2005, Nat, 435, 629

Stinson G. et al., 2011, arXiv e-prints

Stocke J. T., Shull J. M., Penton S., Donahue M., Carilli C., 1995, ApJ, 451, 24

Stocke J. T., Penton S. V., Danforth C. W., Shull J. M., Tumlinson J., McLin K. M., 2006, ApJ, 641, 217

Stocke J. T., Danforth C. W., Shull J. M., Penton S. V., Giroux M. L., 2007, ApJ, 671, 146

Tepper-García T., Richter P., Schaye J., Booth C. M., Dalla Vecchia C., Theuns T., 2012, preprint (arXiv:1201.5641)

Theuns T., Leonard A., Efstathiou G., 1998a, MNRAS, 297, L49

Theuns T., Leonard A., Efstathiou G., Pearce F. R., Thomas P. A., 1998b, MNRAS, 301, 478

Theuns T., Leonard A., Schaye J., Efstathiou G., 1999, MNRAS, 303, L58

Theuns T., Viel M., Kay S., Schaye J., Carswell R. F., Tzanavaris P., 2002, ApJ, 578, L5

Tikhonov A. V., Klypin A., 2009, MNRAS, 395, 1915

Tilton E. M., Danforth C. W., Shull J. M., Ross T. L., 2012, arXiv e-prints

van de Weygaert R., van Kampen E., 1993, MNRAS, 263, 481

Wakker B. P., Savage B. D., 2009, ApJS, 182, 378

Wiersma R. P. C., Schaye J., Smith B. D., 2009a, MNRAS, 393, 99

Wiersma R. P. C., Schaye J., Theuns T., Dalla Vecchia C., Tornatore L., 2009b, MNRAS, 399, 574

Williger G. M., Smette A., Hazard C., Baldwin J. A., McMahon R. G., 2000, ApJ, 532, 77

Wilman R. J., Morris S. L., Jannuzi B. T., Davé R., Shone A. M., 2007, MNRAS, 375, 735

Woodgate B. E. et al., 1998, PASP, 110, 1183

APPENDIX A: CHECK FOR SYSTEMATIC EFFECTS

In this appendix, we investigate possible biases or systematic effects that could be present in the data analysis.

A1 Comparison between our subsample and the whole DS08 sample

In this section we explore whether the subsample of H I systems used here is statistically different from the rest of the H I population found in the other sightlines of the DS08 catalogue. For this, we compared the column density (N_{HI}) and Doppler parameter (b_{HI}) distributions between the 106 absorption systems found inside the void catalogue volume ($0.01 \leq z_{abs} \leq 0.102$ in 11 sightlines) with those 545 outside this volume. The KS test gives a probability of

≈5 per cent and ≈90 per cent that both N_{HI} and b_{HI} distributions, inside and outside the void catalogue volume, are drawn from the same parent distribution, respectively. This shows that there is no significant difference in the b_{HI} distribution and an ≈2σ difference between the N_{HI} distributions.

One explanation for such a difference could be due to an intrinsic evolution of the Lyα forest between $z_{abs} \lesssim 0.102$ and $0.102 \lesssim z_{abs} < 0.4$. To check this, we performed a KS comparison between the 286 absorbers at $z_{abs} < 0.102$ (regardless of whether they are inside the void catalogue volume or not) with the 365 systems at higher redshifts, to look for a possible difference in both N_{HI} and b_{HI} distributions. The distribution of b_{HI} does not show any difference (KS probability ≈87 per cent). On the other hand, the KS probability for the two N_{HI} distributions is ≈8 per cent, hinting that such evolution could be present. We, however, note that an observational bias between low- and high-z systems (e.g. due to different selection functions) could also explain the observed difference. We did not further explore this matter.

Finally, we repeated the previous comparisons between the 106 systems inside the void catalogue volume with those 155 outside it having $0.01 \leq z_{abs} \leq 0.102$. The KS test gives this time a probability of ≈23 per cent and ≈81 per cent of both N_{HI} and b_{HI} inside and outside the void catalogue volume are drawn from the same parent distribution, respectively. No significant (>2σ) differences are found for these samples. Thus, we conclude that the properties of the systems in the sightlines used in this work are not statistically different from the properties of the systems in other sightlines when we restrict ourselves to the same redshift range.

We note that for our comparisons we use systems with N_{HI} below the completeness of the column density distribution itself ($N_{HI} \lesssim 10^{13.4}$ cm^{-2}). The classification of absorber environment does not depend on column density but rather corresponds to a geometrical association of absorbers with known galaxy voids. Therefore, this should not affect any of our results. We also checked that none of the AGNs used here were observed in particular for having sightlines intersecting a known void region.

A2 Systematics in the DS08 characterization method

A particular source of concern is the fact that DS08 used different methods for obtaining the H I column densities and Doppler parameters in the catalogue. They used COG solutions when other Lyman series lines were available other than Lyα. For the rest of the systems, they used either a single Voigt profile fit (preferentially for strong or blended lines) and/or the AOD method (Savage & Sembach 1991, preferentially for weak, asymmetric or noisy lines). We will refer to these as Lyα-only methods. Given that we have been using systems without distinction between these different methods, we will explore any possible bias that this could produce.

Fig. A1 shows H I column densities versus H I Doppler parameters for the 106 systems in our sample, where the different characterization methods used by DS08 are shown in different colours/symbols. It is possible to observe a clear separation between column densities derived from Lyα-only methods and COG solutions. This difference is a direct consequence of the fact that COG solutions can only be obtained for systems showing a high-order Lyman series line, whose equivalent widths are smaller than Lyα for the same N_{HI} and b_{HI} values (because they have smaller wavelengths and smaller oscillator strengths). This results in a shift of the completeness level to higher column densities for the COG solutions, as can be seen in Fig. A1. On the other hand, no significant difference seems to be
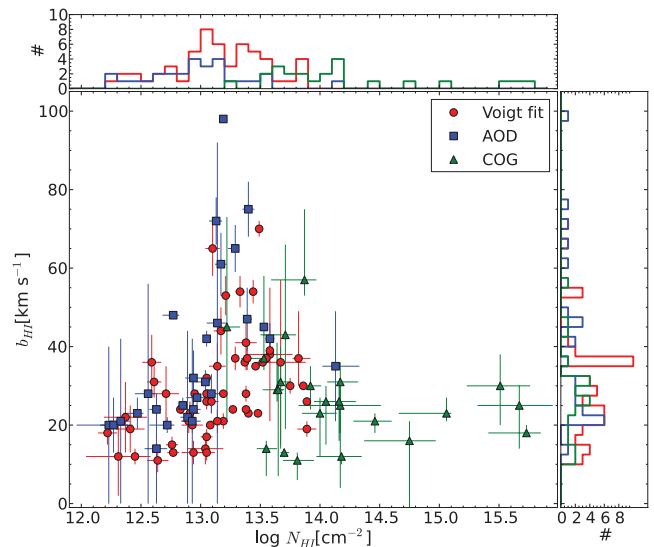
Figure A1. H I column density versus H I Doppler parameter for systems in our sample. Different characterization methods (see Section A2) are shown by different colours/symbols. Red circles correspond to systems measured by Voigt profile fits. Blue squares correspond to systems measured by the AOD method. Green triangles correspond to systems measured by a COG solution. Histograms (arbitrary binning) are also shown around the main panel using the previous colour definition.

present for b_{HI} values between different characterization methods, which has been confirmed by the KS test.

Our definitions of the different LSS samples do not depend on either N_{HI} or b_{HI} but rather correspond to a geometrical selection of how far away a system lies from the centre of a void. Thus, the aforementioned difference observed in N_{HI} should not affect the conclusions drawn from this study as long as our different LSS samples have similar contributions of systems measured with one method or the other. Assuming a Poisson distribution for the number of systems in each sample, there is a relative contribution of 82 ± 18 per cent (82 ± 18 per cent), 73 ± 17 per cent (74 ± 17 per cent) and 82 ± 30 per cent (79 ± 27 per cent) for systems measured by either Voigt fit or AOD methods in the void, void-edge and unclassified samples, respectively. These numbers are all consistent with each other within 1σ. Therefore, we conclude that different characterization methods do not introduce an important bias in our analysis.

There is also a reported systematic effect seen when using Lyα-only systems by which N_{HI} estimates are typically (with large scatter) low by a factor of ∼3, while b_{HI} are high by a factor of ∼2 (Shull et al. 2000; Danforth et al. 2006). This systematic effect is important for higher column densities. Our sample is dominated by systems with $N_{HI} < 10^{14}$ cm^{-2}, for which the effect is smaller than the quoted numbers (see figs 2 and 3 from Danforth et al. 2006). Therefore, despite the fact that our sample is dominated by Lyα-only measurements, we do not consider this effect to be important. Finally, as previously argued, even if any of these effects are present they will affect each of our LSS samples in roughly the same proportion.

A3 Observables as a function of redshift

We also checked that no bias is present in our samples as a function of redshift. Fig. A2 shows both N_{HI} and b_{HI} values as a function of redshift (middle and bottom panels). Systems belonging to
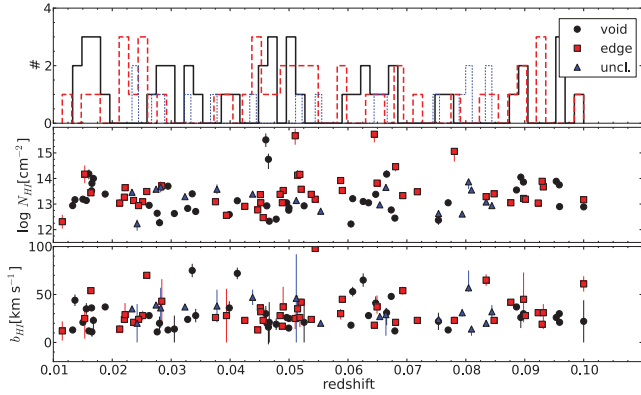
Figure A2. Distribution of observables as a function of redshift. The middle and bottom panels show the distribution of $N_{\rm HI}$ and $b_{\rm HI}$, respectively. Different LSS samples are shown by different colours/symbols: void (black circles), void-edge (red squares) and unclassified (blue triangles). The top panel shows the distribution of different LSS samples as a function of redshift: void (black solid line), void-edge (red dashed line) and unclassified (blue dotted line). For simplicity, we only show LSS definitions based on X.

different LSS samples are shown by different colours/symbols. Both distributions look very uniform across the full redshift range. The top panel shows the distribution of void, void-edge and unclassified absorbers as a function of redshift. The KS test shows no significant difference between these LSS samples. We conclude that there is no evident systematic effect as a function of redshift. For simplicity, we have only used LSS definitions based on X in Fig. A2, but the previous results also hold using D instead.

The catalogue of P12 used a nearly complete, magnitude-limited sample of galaxies to define the voids. Despite this, we performed an independent check by looking at the mean radius $\langle R_{\rm void} \rangle$ as a function of redshift. If the catalogue is well defined, we should expect to have this radius constant across redshift range (assuming no measurable evolution). We confirmed that this is actually the case by dividing the sample in six redshift bins and measuring the mean value. We found that the mean radius is constant with $\langle R_{\rm void} \rangle \approx 13 \pm 3\,h^{-1}$ Mpc in each bin.

This paper has been typeset from a TeX/LaTeX file prepared by the author.